Research Square

Preprints are preliminary reports that have not undergone peer review.
They should not be considered conclusive, used to inform clinical practice,
or referenced by the media as validated information.

Cortical Oscillatory Dynamics Track Sympathetic Arousal and Index Individual Differences in Anxiety

Kristina Pultsina

kpultsin@jyu.fi

University of Jyväskylä https://orcid.org/0000-0001-7128-2832

Ivan Zubarev

Aalto Universty https://orcid.org/0000-0002-1620-8485

Pinja Ronkainen

University of Jyväskylä

Tiina Parviainen

University of Jyväskylä

Article

Keywords:

Posted Date: July 22nd, 2026

DOI: https://doi.org/10.21203/rs.3.rs-10208090/v1

License: This work is licensed under a Creative Commons Attribution 4.0 International License. Read Full License

Additional Declarations: There is **NO** Competing Interest.

Abstract

Phasic sympathetic arousal, indexed by electrodermal activity (EDA), is accompanied by distributed cortical activity, yet which cortical rhythms track these autonomic responses, and when, remains poorly understood hemodynamic imaging has mapped the contributing network but lacks the temporal resolution to resolve this coupling. In 85 adults, we combined magnetoencephalography (MEG) with EDA during a sustained-threat task evoking a graded build-up of arousal. A deep-learning model decoded single-trial sympathetic-response magnitude from whole-brain MEG. Time-resolved liner-mixed effect modelling then showed phasic EDA was preceded by early, overlapping beta synchronization in ventral-visual and posterior-cingulate cortex and gamma synchronization with theta suppression in the right anterior insula, followed by later anterior-cingulate alpha desynchronization. Across individuals, the strength of this oscillation–EDA coupling varied markedly. Critically, anxiety tracked not cortical power or autonomic level alone, but their coupling strength identifying neural–autonomic coupling as a dimension of individual differences in anxiety.

Main

How cortical activity orchestrates the moment-to-moment mobilization of sympathetic arousal during threat remains poorly understood. This question is particularly relevant for understanding how individual differences in brain–body coupling shape the experience of anxiety. While hemodynamic imaging has identified a cortical network including the anterior insula, anterior cingulate cortex, and midline regions associated with the default-mode network as central to autonomic regulation [1–3], its limited temporal resolution has left two critical ambiguities unresolved. First, the temporal ordering of cortical activity within this network relative to sympathetic activation remains unclear. Second, it is unknown which spatiotemporal patterns within it track the magnitude of the autonomic response. Resolving these ambiguities is critical because the nervous system across brain and body form an integrated unit in which autonomic signals both reflect and shape ongoing neural processing [4–6]. This coupling is not merely a means of maintaining homeostatic regulation: autonomic processes contribute to threat monitoring, attentional and decisional weighting, and the preparation of defensive behavior [7–9].

Among emotional states, anxiety is defined by prolonged anticipatory apprehension and uncertainty about potential future harm. It engages sustained mobilization of the sympathetic nervous system, producing physiological changes (including elevated skin conductance, increased heart rate, and altered respiration) that form a core part of the subjective experience of anxious states [10–13]. Individuals differ markedly in the degree to which cortical activity covaries with autonomic responses, and this variability may itself constitute a core neurophysiological dimension of anxiety [14,15]. However, direct evidence linking this cortical–autonomic variability to the experience of anxiety is still lacking a gap that limits our understanding of why some individuals are far more prone to anxiety than others.

Electrodermal activity (EDA) provides a uniquely specific index of sympathetic sudomotor activation[10,16,17], offering a direct measure of transient sympathetic arousal [18]. Converging evidence points to a cortical network including the anterior insula, anterior cingulate cortex, and midline cortical regions associated with the default-mode network as central to autonomic regulation. Activity in these regions covaries with EDA during stressful states [1–3]. However, the majority of this evidence came from hemodynamic imaging, whose temporal resolution limits the ability to resolve the temporal ordering of neural and autonomic events. Consequently, two questions remain unresolved. First, the temporal relationship between cortical activity in this network and sympathetic

activation during threat whether cortical dynamics precede, co-occur with, or follow the autonomic response remains uncharacterized. Second, it remains unclear which neural dynamics within this brain area track the magnitude of the autonomic response, and how individual differences in this coupling relate to the subjective experience of anxiety.

Electrophysiological methods such as EEG and MEG are uniquely positioned to resolve this temporal ambiguity. By providing millisecond temporal resolution and direct access to neural oscillations (rhythmic fluctuations in population-level neuronal activity across large-scale brain networks), these methods enable characterization of neural dynamics at the timescale at which autonomic events unfold [19,20]. A growing body of work links oscillatory dynamics across theta, alpha, beta, and gamma frequency bands to different aspects of autonomic and emotional processes during threat anticipation and aversive learning. Theta-band activity (4–8 Hz), prominently generated in medial prefrontal and cingulate regions, has been associated with threat monitoring and the regulation of defensive responses[21,22]. Alpha oscillations (8–13 Hz), reflecting cortical excitability and attentional gating, have been linked to anticipatory processing and the modulation of arousal states [23,24]. Beta- and gamma-band activity have been implicated in salience processing and the integration of interoceptive signals [25,26]. Critically, recent studies have demonstrated that moment-to-moment fluctuations in oscillatory power can temporally precede EDA responses, indicating that transient neural states co-vary with sympathetic activation on a fine temporal scale and thus may carry information about the magnitude of upcoming autonomic responses, and, in an individually specific manner, the consequent experience of anxiety[27,28].

Previous electrophysiological studies of cortical–autonomic coupling have focused on restricted sets of regions, primarily midline frontal sites [3,28], and predefined frequency bands. This selective approach may overlook distributed cortical contributions from a broader set of regions and across the full frequency range that are likely to contribute to the experience of anxiety. Furthermore, typical paradigms employing brief, discrete stimuli [24,29] do not allow estimation of how cortical-autonomic coupling operates under prolonged and dynamically evolving threat, which more closely resembles real-world anxiety [12,30]. Because autonomic responses arise from coordinated activity distributed across many cortical and subcortical systems, approaches restricted to a few regions or bands are poorly suited to capturing them.

Here, we examined the neural dynamics underlying anticipatory sympathetic arousal using whole-brain source-resolved MEG combined with concurrent phasic EDA recordings during a dynamic escape-game paradigm [31]. Participants continuously monitored and responded to a gradually approaching virtual threat, inducing escalating anticipatory anxiety over extended time periods. Unlike paradigms based on discrete cue–outcome pairings, this design captures sustained threat processing under conditions of ongoing uncertainty and behavioral engagement, more closely approximating the temporal structure of real-world anxiety [30,32]. Autonomic responses are unlikely to be encoded in isolated cortical regions; rather, they emerge from coordinated activity across distributed cortical and subcortical systems representing the cognitive, emotional, and somatomotor aspects of threat processing [4,33,34]. Resolving the spatial, spectral, and temporal structure of this coupling requires methods that handle the high dimensionality of source-resolved MEG data while remaining sensitive to patterns distributed across many regions.

To address these requirements, we adopted a three-stage analytical framework. A spatiotemporal convolutional neural network (LF-CNN[35]) was first trained to estimate single-trial variations in the EDA amplitude from the MEG

source activity preceding the autonomic response. Spatial and temporal features driving successful estimation were then extracted from the model to identify cortical regions and frequency bands of interest. Finally, these regions and bands were taken forward to time-resolved linear mixed-effects modelling (LMEM), which quantified the precise spatial, spectral, and temporal contributions of oscillatory power to variation in EDA magnitude while accounting for inter-individual variability through random-effects structure. This combination allowed us to benefit from both the sensitivity of multivariate pattern analysis and the interpretability of hypothesis-driven inference.

Results

EDA response is modulated by the perceived threat

85 healthy volunteers underwent an escape game task comprising 14 sequences of visual scenes. Each sequence included 4 or 6 scenes depicting running through a maze while being followed by a predator. Each *running scene* (Fig. 1.A) was followed by a static scene of the maze map with locations of the player's avatar and the predator shown on it. The task was designed so that 65% of the sequences ended up with participants getting caught and receiving a mild electric shock.

As expected, the task elicited a robust phasic EDA response shortly after the onset of each *running* scene (Fig. 1c). The EDA response amplitude increased gradually towards the end of the sequence, consistent with the buildup of anticipatory anxiety (Fig. 1b). Within each sequence these amplitude modulations were most prominent between the first scenes (lowest chance of getting a shock) and the last scenes (highest chance of getting a shock) *1.7–3 s* after the scene onset (Fig. 1c). EDA response amplitude within this time interval was positively associated with self-reported unpleasantness (r = 0.223, p-value = 0.038, Fig. 1d) and was used for further analysis.

EDA response amplitude can be predicted from the single-trial MEG signal

A spatiotemporal convolutional neural network [35,36] was trained to predict the single-trial EDA response amplitudes from the source-localized MEG time-courses. MEG epochs of 4.5 s time-locked to each threat scene (–1.5 to 3 s relative to scene onset), spanning the interval before and during the target EDA response, were projected onto individual cortical source spaces, downsampled to 448 compact cortical parcels, and pooled across 85 participants. The LF-CNN model achieved high predictive accuracy, explaining 39.8% of the EDA response variance (R^2 = 0.398 ± 0.04) on the held-out test set (Fig. 2).

A temporally structured cortical oscillatory sequence predicts sympathetic arousal

LF-CNN activation patterns extracted from the model identified distinct spatial and spectral components of the MEG signal which informed successful predictions.

These spatial patterns included bilateral insula, anterior (ACC) and posterior (PCC) cingulate cortices, supramarginal gyrus, superior parietal cortex, and fusiform/ventral visual regions (VVS) (Fig. 2b). Because these

regions were derived from the model rather than defined a priori, we refer to them as data-driven regions of interest (ROIs). ROIs on the medial surface were combined across hemispheres (i.e., not separated into right and left) owing to the spatial resolution characteristics of MEG.

In the spectral domain the model emphasized four frequency bands in the lower theta (3–6 Hz), alpha (7–13 Hz), beta (15–29 Hz), and low gamma (31–39 Hz) frequency ranges (Fig. 2).

To establish when, and in which direction, the model-identified regions and frequency bands contributed to sympathetic arousal, we quantified their coupling with phasic EDA using time-resolved linear mixed-effects modelling (LMEM).

Separate LMEMs were fitted to predict single-trial EDA amplitudes from MEG power estimates at each ROI and frequency band across consecutive 100-ms time windows, allowing for subject-specific baseline EDA levels. Subsequent analyses focused on region–frequency combinations exhibiting significant coupling over time. For these, models were refitted to estimate subject-specific EDA–MEG coupling. This analysis revealed significant trial-by-trial association between fluctuations in cortical oscillatory power and the amplitude of the subsequent EDA response in visual, parietal, insular, and cingulate ROIs.

Coupling between cortical source power and phasic EDA showed pronounced spatial, spectral, and temporal specificity (Table 1, Fig. 3). Specifically, greater early increases in beta power in posterior ROIs (PCC and VVS) and enhancement of gamma activity in the right insular cortex were associated with larger EDA response amplitudes. These early positive effects were followed by reduced theta power in the insula and lower alpha power in the ACC, both of which were also associated with larger EDA response amplitudes. These effects are summarized in Table 1 and Fig. 3.

Table 1
Cortical–autonomic coupling: LMEM results

ROI, hemi	Frequency band, Hz	Time-window, s	F	df (1,2)	p-value
VVS, lh	15–29 Hz	0.1–0.7	*20.9*	*(1,74)*	*< 0.001*
PCC, lh + rh	15–29 Hz	0.0–0.9	*10.1*	*(1,75)*	*0.002*
Insula, rh	31–39 Hz	0.2–0.7	*6.5*	*(1,61)*	*0.013*
Insula, rh	3–6 Hz	0.3–0.7	6.6	*(1,58)*	*0.013*
ACC, lh + rh	7–13 Hz	1.1–1.6	*8.9*	*(1,77.5)*	*0.004*

Neural–autonomic coupling explains individual differences in anxiety

Subject-specific slope estimates from the LMEMs were used as a proxy for the individual neural–autonomic coupling strength. A positive slope indicates that increases in oscillatory power in a specific frequency band within a given ROI were associated with larger phasic EDA responses for that participant; a negative slope indicates the inverse relationship. To examine whether the degree of this coupling was related to dispositional

and state anxiety, Spearman correlations were computed between individual slopes and scores from the State-Trait Anxiety Inventory (STAI), separately for trait anxiety and for state anxiety, the latter assessed both before (S1) and after the experiment (S_2). These analyses were restricted to the specific region–frequency combinations that showed significant time-resolved neural–autonomic associations (Table 2, Fig. 4).

Table 2
Correlation analysis between cortical–autonomic coupling (individual slopes) and anxiety

ROI	Frequency band	Trait anxiety (STAI-T)			State anxiety, pre (STAI-S_1)			State anxiety, post (STAI-S_2)		
		rho [95% CI]	***p***	***q***	***rho [95% CI]***	***p***	***q***	***rho [95% CI]***	***p***	***q***
VVS	15–29 Hz	**-0.27 [-0.45, -0.06]**	**0.011**	**0.044**	-0.03 [-0.27, 0.19]	0.758	0.758	0.07[-0.15, 0.29]	0.489	0.489
PCC	15–29 Hz	-0.08 [-0.33, 0.11]	0.276	0.276	-0.06 [-0.27, 0.16]	0.608	0.758	**-0.30** [-0.49, -0.09]	**0.005**	**0.020***
Insula	31–39 Hz	0.08 [-0.13, 0.30]	0.085	0.117	0.05 [-0.16, 0.27]	0.623	0.758	**0.27** [0.08, 0.47]	**0.011**	**0.020***
Insula	3–6 Hz	0.19 [-0.04, 0.39]	0.088	0.117	0.04 [-0.18, 0.26]	0.695	0.758	**0.26** [0.04, 0.46]	**0.015**	**0.020***

Table 3
Hyperparameter search grid and cross-validated optimal values for the LF-CNN model used to estimate single-trial EDA amplitude from MEG source activity.

Parameter	Grid values	Selected value
Number of components	16, 32, 64, 128	64
Kernel size	8, 16, 32	32
Dropout rate	.05, .075, .1, .2, .33, .5	0.075
L1 regularization	3e-4, 1e-4, 3e-5, 1e-5, 3e-6	1e-5
Pooling window	16, 24, 32, 768	768
Pooling type	max, avg	-

Two distinct patterns emerged across anxiety measures: trait anxiety was negatively associated with coupling strength in posterior visual regions, whereas state anxiety assessed after the experiment was associated with

stronger insular gamma coupling but attenuated insular theta and PCC beta coupling.

In the VVS, individual differences in beta-band coupling strength were negatively correlated with *trait* anxiety (rho = − 0.27, q = 0.044; Fig. 4A). At the group level, greater beta-band power in the VVS was associated with larger EDA responses (i.e., a positive slope). However, this relationship was attenuated in individuals with higher trait anxiety — that is, participants reporting greater dispositional anxiety showed weaker co-variation between beta-band power fluctuations in the ventral visual stream and sympathetic arousal.

A different pattern emerged for *state* anxiety. Significant associations were observed exclusively with *state anxiety collected at the end of the experiment*, suggesting that the task rendered individual differences in cortical–autonomic coupling more behaviorally relevant. In the PCC, beta-band coupling strength was negatively associated with post-experiment state anxiety (rho = − 0.30, q = 0.020; Fig. 4): individuals reporting higher state anxiety after the task showed weaker co-variation between PCC beta-band power and phasic EDA, indicating that PCC beta activity tracked autonomic responses less tightly in participants experiencing heightened anxious states.

In the insula, both gamma-band (rho = 0.29, q = 0.020; Fig. 4B) and theta-band (rho = 0.27, q = 0.020; Fig. 4C) power-to-EDA coupling strengths were positively associated with post-experiment state anxiety. Because the group-level slopes for these two bands were of opposite sign (positive for gamma, negative for theta), the individual-difference correlations indicate distinct effects. Highly state-anxious individuals showed stronger positive coupling between insular gamma power and phasic EDA, but weaker (less negative) coupling between insular theta power and phasic EDA, indicating that trial-by-trial fluctuations in insular theta power tracked sympathetic responses less tightly in these individuals. The two insular bands therefore showed opposite individual-difference profiles: amplified gamma–EDA coupling and attenuated theta–EDA coupling in highly anxious individuals.

In contrast to these coupling effects, mean oscillatory power extracted from each ROI showed no significant association with either trait or state anxiety in any region (all |rho| < 0.11, all p > 0.33). Similarly, phasic EDA amplitude itself was not significantly associated with either state anxiety (rho = 0.17, p = 0.06) or trait anxiety (rho = 0.15, p = 0.119).

Discussion

In this study, we characterized how the spatial, spectral, and temporal dimensions of cortical activity contribute to the emergence of sympathetic arousal during sustained threat, and whether individual variability in this brain-to-body coupling is relevant to anxiety experience. We used a data-driven deep learning framework to identify cortical regions and oscillatory features of the MEG signal predictive of upcoming sympathetic responses indexed by EDA, then used confirmatory time-resolved mixed-effects modeling to quantify these contributions while accounting for inter-individual variability. Three principal findings emerged. First, sympathetic arousal was preceded by temporally structured oscillatory dynamics spanning sensory, contextual, and salience-related cortical systems, indicating that autonomic responses are associated not with a single region or frequency band, but with the coordinated engagement of distributed cortical areas. Second, the strength of these neural–autonomic interactions varied substantially across participants. This variability was reliably related to individual

differences in anxiety, both as a stable trait and as a state modulated by the experimental context. Third, anxiety showed no association with any specific pattern of cortical activity or autonomic responsiveness alone, but with the strength of coupling between the two. This suggests that anxiety may be better understood as a shift in how cortical dynamics co-vary with bodily arousal rather than as an elevation in either domain alone. This level of characterization, linking brain–body coupling to meaningful variation in human anxiety experience, became accessible only by jointly resolving the spatial, temporal, and spectral structure of neural–autonomic interaction.

The early rise in EDA, accompanied by beta-band synchronization in the VVS and PCC shortly after the threat-predictive scene onset, aligns with the role of beta oscillations in maintaining the current cognitive set and supporting top-down, predicted states. Thus, in the ventral visual stream, beta synchronization may reflect the retention of threat-relevant representations [37,38]and heightened alertness and attentional engagement [39] covarying more tightly with the autonomic response. The PCC, in turn, is a hub of the default-mode network involved in internally directed and contextual information processing [40,41]. Greater beta synchronization in the PCC may reflect a higher degree of internalizing the threat context keeping the impending danger in mind and was accompanied by greater autonomic mobilization.

In the right anterior insula, threat anticipation was marked by a pattern of early gamma-band synchronization followed by a suppression of theta-band power. Both spectral changes were strongly associated with larger phasic EDA responses. The anterior insula is recognized as an integrative hub that receives continuous interoceptive information and flags salient changes, and its activity has been linked to autonomic responses [42,43]. The specificity to the right anterior insula is consistent with the proposed right-hemisphere lateralization of sympathetic-related processing and the representation of negative affective body states [44]. Greater gamma synchronization likely reflects enhanced local neuronal firing and network binding in the insula [45], consistent with the representation of salient interoceptive signals and covarying with phasic EDA. Consistent with this, intracranial recordings have shown that human anterior insula gamma power increases during aversive stimuli and correlates with elevated skin conductance [46]. The subsequent suppression of theta rhythms in the same region is in line with recent evidence linking prefrontal theta suppression to sympathetic activity [47]. Theta oscillations support network coupling and integrative control [48,49]; reduced insular theta may therefore index a release of these circuits from an integrative mode, accompanying a shift toward urgent stimulus processing. Thus, the combined pattern of early gamma-band increase and theta-band suppression in the right insula is consistent with a two-phase profile initial amplification of interoceptive salience followed by a release from tonic integrative processing that together covaried with larger phasic EDA responses.

In the ACC, alpha-band oscillatory dynamics were inversely related to EDA responses. Approximately 1.1–1.6 s after stimulus onset, alpha power suppression in the ACC predicted greater phasic EDA. The ACC plays a central role in evaluating motivational significance and coordinating autonomic adjustments in response to salient events [4,50]. Alpha desynchronization reflects increased cortical engagement and reduced inhibition; the inverse relationship with EDA suggests that as the ACC becomes more actively engaged with the threat context, stronger autonomic responses follow.

Taken together, the identified neural correlates of sympathetic arousal were temporally structured. Posterior beta-band synchronization (VVS and PCC) together with insular gamma synchronization and concurrent theta suppression occupied largely overlapping early windows (spanning 0.0–0.9 s), consistent with rapid encoding of the threat-predictive visual cue, contextual appraisal, and a near-simultaneous engagement of interoceptive

salience processing. Alpha desynchronization in the ACC emerged substantially later (1.1–1.6 s), consistent with a subsequent evaluative stage. Because these effects were defined by the intervals over which oscillatory power covaried with EDA rather than by estimated onset latencies, we do not interpret the relative timing of the early, overlapping effects as a fixed processing order. The data instead indicate that sympathetic arousal during threat anticipation is associated not with a single region but with the temporally distributed engagement of multiple cortical systems an early, partially concurrent involvement of sensory and interoceptive areas followed by a later cingulate contribution.

Critically, our large dataset allowed us to pinpoint marked individual variation in how neural activity co-varied with sympathetic output, and these individual coupling strengths systematically related to anxiety experience. Importantly, these effects were not explained by baseline neural power or overall, EDA amplitude; instead, they reflect differences in how strongly specific oscillatory signals in specific cortical systems are associated with autonomic responses. Individuals with higher trait anxiety showed reduced coupling between beta-band activity and EDA. Beta rhythms often accompany stabilized cortical states, integration of contextual information, and maintenance of task structure [51]. A reduced beta–EDA coupling slope suggests that autonomic output is less closely integrated with the cortical states underlying threat perception in anxious individuals. This interpretation aligns with observations that anxiety is associated with diminished use of contextual cues, reduced capacity to modulate arousal through cortical processing, and greater difficulty integrating situational information when evaluating threat[12,52,53].

The picture was different for the immediate experience of anxiety. Whereas trait anxiety was expressed mainly through coupling in ventral visual regions, the experienced level of anxiety was modulated by cortical–EDA coupling in the insula, pointing to a role for interoceptive processing and salience attribution in the momentary experience of anxiety. The stronger insular gamma–EDA coupling in individuals who experienced the task as more anxiety-evoking is in line with the role of gamma synchronization in local salience signaling and rapid interoceptive flagging [45,54,55]. A steeper gamma–EDA coupling slope indicates that fluctuations in this fast, focal salience signal co-vary more tightly with sympathetic output in individuals experiencing heightened state anxiety, consistent with amplified emotional and interoceptive responsivity [15,56] and with evidence that more anxious individuals show amplified autonomic correlates of affective neural responses [57,58]. The insular theta finding showed the opposite individual-difference profile. At the group level, threat-related insular theta desynchronization tracked larger EDA responses, consistent with theta's role in network integration and tonic integrative control [48,49]; release from this integrative mode is thought to facilitate a shift toward urgent stimulus processing. When the experienced anxiety was high, however, this theta–EDA covariation was attenuated, indicating that the integrative-release component of the insular response failed to track autonomic output as tightly. The simultaneous amplification of gamma coupling and attenuation of theta coupling in state-anxious individuals therefore points to a partial dissociation within the canonical insular dual response: the local, focal salience component (gamma) is heightened, while the network-integrative component (theta) is decoupled from arousal. This attenuation need not reflect a failure of brain–body coupling; it may instead represent a functional outcome for example, an active attempt to down-regulate the unpleasant feeling of anxiety and the present design cannot adjudicate between these accounts.

The negative association between PCC beta–EDA coupling and experienced anxiety represents a complementary pattern, likely reflecting a loss of top-down contextual control over autonomic output. Because PCC beta synchronization normally supports contextual stabilization, predictive signaling, and the maintenance

of task-relevant representations[25,51], its weaker coupling in more state-anxious individuals indicates that the cortical signals normally engaged in contextual stabilization become decoupled from bodily arousal. This parallels the trait-anxiety effect observed in the VVS: in both regions, posterior beta-band signals normally linked to stabilizing or contextual processing lose their dynamic coordination with autonomic responses as anxiety increases.

The differential association of coupling strength with trait versus state anxiety across regions deserves note. Beta–EDA coupling in the VVS was specifically associated with trait anxiety, a stable dispositional characteristic [12,59]. In contrast, gamma-EDA and (in the opposite direction) theta–EDA coupling in the insula, as well as beta-EDA coupling in the PCC, were associated with the experienced level of anxiety after the task. This dissociation suggests that perceptual and contextual brain–body coupling may index long-standing vulnerability[12,53], while interoceptive and default-mode coupling more closely tracks fluctuating anxiety states elicited by the immediate situational context [15,44]. One possibility is that acute state anxiety links most strongly with local network interactions in interoceptive circuits, whereas stable trait-level vulnerability is reflected in beta-band coupling consistent with more top-down, stabilizing cortical influences. Across both measures, reduced beta-band coupling accompanied higher anxiety trait anxiety in the ventral visual stream and state anxiety in the PCC consistent with the proposed role of beta power in maintaining predicted, contextual states: as anxiety rises, these posterior beta signals appear to lose their grip on autonomic output.

Notably, neither mean oscillatory power nor overall phasic EDA amplitude showed significant associations with anxiety scores. This null finding is informative: it suggests that anxiety is not straightforwardly indexed by the level of neural activity or the magnitude of autonomic responses in isolation [57,60]. Rather, the present results suggest that the dynamic co-variation between neural and autonomic signals is the key dimension along which anxiety-related individual differences emerge. This is consistent with a view of anxiety as a disruption in brain–body communication rather than a simple change in neural or physiological reactivity per se [4,6].

Within the broader literature on emotion and autonomic control, the present findings support a model in which sympathetic arousal is shaped by the dynamic interplay of two classes of cortical processes: stabilizing, contextual processes indexed here by posterior and default-mode beta synchronization, and arousal-potentiating salience processes indexed by insular gamma activity. Trait anxiety appears to be characterized by alterations in this interplay specifically, a weaker link between contextual stabilizing signals and autonomic output whereas state anxiety is accompanied by amplified co-variation of focal salience signals with physiological engagement. In other words, the dispositional tendency to experience anxiety may be driven by an uncoupling between physiological representations of threat and the cognitive-contextual regulation of these representations. Critically, this understanding emerged only because the present analytical approach jointly resolved the spatial, temporal, and spectral structure of neural–autonomic coupling, capturing distributed patterns of brain–body interaction that would remain invisible when any single dimension is examined in isolation. It is this multidimensional characterization that allowed individual differences in coupling to be linked to meaningful variation in anxiety experience, bridging the gap between fine-grained neurophysiological dynamics and the lived reality of how people differently experience threat and uncertainty. This interpretation aligns with evidence from neuroimaging, psychophysiology, and lesion studies showing that anxiety involves both reduced cortical regulation of autonomic output and enhanced responsivity to threat-related internal cues [60–62].

Strengths and limitations

One limitation should nonetheless be noted: the present observational design captures time-resolved associations rather than causal mechanisms. Although the neural oscillatory patterns temporally preceded the sympathetic responses, our design cannot establish the direction of this relationship, and we therefore interpret all findings in terms of temporal covariation and coupling rather than directional or causal influence.

Conclusion

By combining deep-learning decoding of single-trial sympathetic responses with confirmatory time-resolved modelling, this study identifies temporally progressing oscillatory signatures that precede sympathetic arousal during threat and demonstrates that the strength of cortical–autonomic coupling, rather than either cortical or autonomic signaling alone, varies systematically with experience of anxiety. Anxious individuals show a shift from integrative, contextual brain–body coupling toward focal, salience-driven coupling reflected in weaker coupling of posterior beta-band and insular theta activity to autonomic output, alongside stronger coupling of insular gamma activity. These findings provide a window onto how cortical dynamics co-vary with bodily arousal and highlight neural–autonomic coupling as a potential marker of dimensional variation in anxiety experience.

Methods

Participants

The study included 92 neurotypical participants aged 18 to 56 years (66 females, 26 males; M = 29.33, SD = 8.94). Two were excluded due to noisy EDA recordings in more than 50% of their runs. Two were excluded because of a technical error during the experiment that caused the final runs to be lost. Three were excluded due to excessive noise in the MEG recordings. The final sample comprised *85 participants*.

Data were collected between 2024 and 2025. Participants were recruited through recruitment emails distributed via university mailing lists, online advertisements posted on University of Jyväskylä (JYU) websites, and word-of-mouth referrals. Although most participants were university students, the online recruitment channels also reached individuals from across Finland. Inclusion criteria were as follows: age between 18 and 60 years; normal or corrected-to-normal vision; absence of any diagnosed severe psychiatric disorder (e.g., major depressive disorder); no neurological illness or use of medication affecting the central nervous system; and no metal implants incompatible with MEG recording. Individuals with severe psychiatric conditions were excluded to minimize potential risk to those with pre-existing psychological vulnerability.

The study protocol was approved by the Ethics Committee of the University of Jyväskylä, and all the study procedures were conducted in accordance with the Declaration of Helsinki. All participants provided written informed consent prior to participation. Participants were free to discontinue the experiment at any point, and the researchers continuously monitored participants' well-being, terminating the session if required. After the experiment, participants were debriefed.

Experimental Procedure

The experimental task was adapted from the escape game paradigm described by (Fung et al., 2019), developed to elicit autonomic arousal through prolonged anticipation of threat. In this paradigm, participants navigate an

environment while being pursued by a predator, a context known to engage defensive survival circuits and anticipatory anxiety. The task was performed with simultaneous MEG and electrodermal activity (EDA) recording.

The experimental task comprised 14 game rounds (blocks). Each round included sequence of scenes, during which participants were shown a video of running through a maze. Each of these running scenes was followed by one of the two following conditions scenes. First, the participant's avatar location appeared on the map in red, indicating that they had 1.5 seconds to decide the next direction. Alternatively, participants' avatar appeared in blue, and they observed the predator's avatar approaching. Each block included four or six of these alternating running and map scenes, ending in either escaping or getting caught by the predator. Regardless of participants' choices the experiment was designed in 65% of the blocks they got caught and received a mild electric shock (ES) applied to the right ring finger using two ring electrodes. Stimulation strength was adjusted for each participant individually before the experiment.

After each round, participants rated their subjective anxiety, intensity, and pleasant/unpleasant feelings on a scale from 0 to 7. In addition, trait and state anxiety were estimated by State-Trait Anxiety Inventory (STAI) [59]. The state anxiety was assessed twice before and after the experiment.

In contrast to classical Pavlovian threat-conditioning paradigms, where aversive outcomes are time-locked to discrete cues and participants have no active role, the escape game paradigm involves ongoing navigation under the possibility of threat. The outcome (electric shock) is not directly tied to participants' decisions, which maintains uncertainty throughout each epoch. This design leads to gradual build-up of anticipatory arousal, making it particularly suitable for studying the dynamic interactions between EDA and the cortical activity measured by MEG.

Electrodermal response recording and processing

The EDA was recorded using Ambu electrodes (NEUROLINE 710) placed on the medial plantar surface of the right foot. The EDA signal was segmented into epochs from − 2.0 to 6.0 s relative to the onset of each running phase and was preprocessed using the NeuroKit software [63]. After low-pass filtering with a 4th-order Butterworth filter (3 Hz cutoff), the EDA signal was decomposed into tonic and phasic components, and subsequent analyses were performed on the phasic component [64]. Phasic EDA was z-scored within each participant.

MEG data acquisition

Brain activity was recorded using a 306-channel whole-head Elekta TRIUX MEG system (Megin Oy, Helsinki, Finland) in a magnetically shielded room. Data were sampled online at 1000 Hz with a hardware band-pass filter of 0.03–330 Hz. Before each recording session, five head position indicator (HPI) coils were affixed to the participant's scalp three across the forehead and one behind each ear. Their positions, together with three anatomical fiducial points (the nasion and the left and right preauricular points), were then registered using a 3-D digitizer to allow co-registration of the head with the MEG sensor array.

MRI data acquisition and preprocessing

All participants underwent magnetic resonance imaging (MRI; 1.5 T, voxel size 1 mm x 1 mm x 1 mm). The T1-weighted images were processed with the FreeSurfer's (v.6.0.0) default 'recon-all' pipeline [65]. Its main included

steps were motion correction, spatial normalization, skull stripping, gray/white matter segmentation.

MEG preprocessing and source localization

We applied the temporal signal space separation method (tSSS) [66] to the raw data using MaxFilter (Elekta Neuromag software). For further offline analysis, MNE-Python software was used [67]. We removed cardiac artifacts and artifacts related to eye movements from continuous data using the 'fastICA' method implemented in MNE-Python software [68]. Specifically, we excluded contaminated epochs by thresholding the mean absolute signal values filtered above 70 Hz from each channel below 7 standard deviations of the average across the channel. MEG data were filtered using a notch filter at 50 Hz and bandpass filtered at 0.1 to 90 Hz.

The raw data was resampled to 500 Hz. Myogenic artifacts were detected using the MNE-Python function *'annotate_muscle_zscore'* with threshold = 5. Data periods contaminated with automatically detected movement and myogenic burst artifacts were excluded from further analysis. The data were segmented into epochs from −1.5 to 6.0 s relative onset of each running scene.

MEG data were co-registered with the structural MRI of the head, and a 3-layer boundary element model was constructed. We then created surface-based source space with 4096 vertex sources in each hemisphere and estimated the forward solution. Noise covariance matrices were estimated using 5-minute empty room measurements taken prior to the experiment. The inverse solution was estimated using the following parameters: dipole orientation constrained to be orthogonal to the cortical surface (loose parameter set to 0.2), depth weighting parameter of 0.8, and signal-to-noise ratio set to 1. The source activity estimated using sLoreta [69].

Each source-reconstructed source space was subsequently divided into contiguous cortical parcels of approximately equal size using the *'aparc_sub'* parcellation[70]. The parcellations were morphed onto the individual cortical surfaces using the *'mne.morph_labels'* function.

In the identified regions of interest, a time–frequency analysis using Morlet wavelets was performed across the main frequency bands: theta (3–6 Hz, n cycles = 2), alpha (7–13 Hz,n cycles = 4), beta (15–29 Hz,n cycles = 4), and gamma (31–39 Hz, n cycles = 7). Individual baseline for each epoch with additional log10-transformation was applied.

Predictive neural regression

Spatiotemporal convolutional neural network (LF-CNN [35]) was trained to predict trial-to-trial variations in the EDA response by minimizing a Mean-Squared Error (MSE) loss function. The input to the network comprised single-trial time courses (n = 3600) of 448 cortical sources in the 4.5s time window before the EDA response (-1.5–3.0s relative to the task onset). These inputs were down-sampled to 200 Hz to reduce the computational load and prevent overfitting. Prediction target was defined as relative EDA amplitude change to the EDA amplitude at the start of each experimental block.

Data from all trials and all participants were pooled together and split into 10 folds. Model performance was estimated using a nested cross-validation scheme where on each fold the model was trained on 80% of the data, 10% of the data was used as a validation set used for tracking model convergence and early stopping. Out-of-sample performance was estimated on the remaining 10% of the data (holdout test set). We report average

mean-squared error and R2 score across the folds of the cross-validation, as well as the same metrics, evaluated on the holdout after each training fold. Thus, the test set metrics comprise average out-of-sample performance over 9 model initiations.

Each training epoch comprised 500 training steps performed on mini-batches of 50 MEG epochs. The model was trained using Adam optimizer with a learning rate of 3*10 − 4 until the early stopping criteria were met i.e. the validation loss did not decrease for 10 consecutive training epochs. After the training was complete the model was restored to the state yielding minimal validation loss and evaluated on the test set. The hyperparameter search was performed using the parameter grid described in Table 3.

Predictive pattern analysis

To investigate brain regions and oscillatory patterns that allowed the model to predict modulations of the EDA response, we explored activation patterns that had the most prominent contribution to predictions. To that end a single spatiotemporal component explaining the largest proportion of variance was selected following the procedure described Zubarev et al., 2019[35].

Source-space activation patterns of each component were obtained by multiplying the weights of the spatial filter by the source covariance matrix [71] of the validation fold. This procedure was repeated 10 times for each cross-validation fold to obtain the grand-average source activation pattern. Regions of interest were obtained by identifying the top 10th percentile of the most active cortical sources in the grand-averaged spatial activation pattern.

This procedure resulted in the retention of 41 cortical sources. To confirm that these sources carried the information used by the network, we retrained the model using only their time-courses. This ROI-restricted model achieved $R^2 = 0.231 \pm 0.04$ on the validation set and $R^2 = 0.138 \pm 0.04$ on the test set, thereby recovering approximately 46% and 34%, respectively, of the variance explained by the full model.

Similarly, informative frequency bands were obtained by exploring the frequency response of the temporal convolution kernels (Fig. 2). We compared relative power spectra (RPS) of the network activations before and after the temporal convolution layer and identified contiguous frequency bands where output was reliably amplified compared to input. This procedure was repeated for each fold separately and averaged across folds. The resulting RPS are shown in Fig. 2.

ROIs and frequency bands identified as informative by the Deep Learning model were then used for post-hoc interpretation analysis using Linear Mixed Effects Model (LMEM) (Bates et al., 2015).

Time–Frequency MEG Features Predicting EDA

The association between trial-to-trial modulations of MEG activity in the identified ROIs and the phasic EDA response was probed using a two-stage linear mixed-effects approach[72]. In a first, time-resolved stage, we identified the time interval during which MEG power significantly predicted the EDA response. In a second, confirmatory stage, MEG power was averaged within this predictive interval and used to fit a stricter random-slope model, providing validation of the time-resolved findings and yielding subject-specific estimates of MEG–EDA coupling strength. Both stages were estimated separately for each ROI and frequency band of interest. This

design allowed us to investigate whether changes in oscillatory power were significantly associated with the magnitude of the EDA response while explicitly accounting for individual differences.

Stage 1: Time-resolved analysis. We first identified the time interval in which MEG power best predicted the phasic EDA response by fitting a linear mixed-effects model separately at each 100-ms MEG time bin relative to stimulus onset. For each time bin, the phasic EDA response on trial *i* of subject *j* was modelled as:

$$EDA_{ij} = \beta_0 + \beta_1 \bullet \ MEG\ power_{ij} + \alpha_{0j} + \epsilon_{ij}$$ **(1)**,

where *β*0 is the fixed-effect intercept, *β*1 is the fixed-effect slope quantifying the instantaneous coupling between MEG power and the EDA response, *α*0j is the subject-specific random intercept, and *ε*ij is the residual error. Both the dependent and independent variables were z-scored across the full dataset before model fitting, and models were estimated using restricted maximum likelihood (REML). Inference on *β*1 was performed using cluster-robust standard errors (CR2 estimator), with subject as the clustering unit and Satterthwaite-approximated degrees of freedom, as implemented in the *clubSandwich* R package[73,74]. Ninety-five percent confidence intervals were computed as the slope estimate ± 1.96 × SE. The resulting time course of *β*1 was used to determine the MEG time interval during which MEG power significantly predicted the EDA response, with p-values corrected for multiple comparisons across time bins using the Benjamini–Hochberg false discovery rate [75].

Stage 2: Confirmatory random-slope analysis. To derive subject-specific coupling estimates and to validate the time-resolved finding under a stricter model, we collapsed the predictive interval identified in Stage 1 to a single value per observation by averaging MEG power within that window. The trial-level phasic EDA response was then modelled as:

$$EDA_{ij} = \beta_0 + \beta_1 \bullet \ MEG\ power_{ij} + \alpha_{0j} + \ \alpha_{1j} + MEG\ power_{ij} \bullet \alpha_{0j} + \epsilon_{ij}$$ **(2)**,

where *α*0j and *α*1j are the subject-specific random intercept and random slope on MEG power, respectively, jointly drawn from a bivariate normal distribution with covariance matrix *Σ*. By explicitly allowing each participant's coupling slope to vary, this specification requires any population-level MEG–EDA association to hold above and beyond inter-individual heterogeneity in coupling strength, making it more conservative than the random-intercept-only Stage 1 model. A fixed-effect slope *β*1 that survives this structure therefore reflects an effect that is robust to between-subject variation in coupling, while the subject-specific random slopes themselves provide the individual coupling estimates carried forward to the correlation analyses below. Ninety-five percent confidence intervals for *β*1 were obtained from 1,000 parametric bootstrap iterations.

Subject-specific slope estimates (*β*1 + *α*1j) were obtained as the best linear unbiased predictors (BLUPs) of the random slope plus the fixed-effect slope, i.e., the per-subject expected change in EDA per unit increase in MEG power within the predictive window. Deriving these slopes from the pre-selected predictive MEG window ensured that individual-difference analyses were constrained to a physiologically meaningful interval, thereby avoiding circular inference and further reducing the Type I error.

These subject-specific slopes provided a quantitative index of each participant's coupling strength, which was subsequently used in individual-difference analyses examining associations with trait and state anxiety measures. For each ROI–frequency combination that survived the time-resolved analysis, we computed

Spearman rank correlations between the individual slope estimates and three anxiety scores: trait anxiety (STAI-T), pre-experiment state anxiety (STAI-S1), and post-experiment state anxiety (STAI-S2). Ninety-five percent confidence intervals for each Spearman ρ were obtained from 5,000 percentile bootstrap resamples (*boot* package[76]). To control for multiple testing, p-values were adjusted using the Benjamini–Hochberg false discovery rate, applied separately within each anxiety measure across the four ROI–frequency combinations entered the analysis (VVS beta, PCC beta, insular gamma, and insular theta).

Declarations

Funding

The project was supported by Business Finland (grant “DIGIMIND” 7981/31/2022).

References

1. Beissner F, Meissner K, Bär KJ, Napadow V (2013) The autonomic brain: An activation likelihood estimation meta-analysis for central processing of autonomic function. J Neurosci 33
2. Critchley HD, Elliott R, Mathias CJ, Dolan RJ (2000) Neural activity relating to generation and representation of galvanic skin conductance responses: A functional magnetic resonance imaging study. J Neurosci 20
3. Nagai Y, Critchley HD, Featherstone E, Trimble MR, Dolan RJ (2004) Activity in ventromedial prefrontal cortex covaries with sympathetic skin conductance level: A physiological account of a ‘default mode’ of brain function. *NeuroImage* 22
4. Critchley HD, Harrison NA (2013) Visceral Influences on Brain and Behavior. *Neuron* 77
5. Damasio AR (1996) The somatic marker hypothesis and the possible functions of the prefrontal cortex. Philos Trans R Soc B Biol Sci 351
6. Thayer JF, Lane RD (2000) A model of neurovisceral integration in emotion regulation and dysregulation. J Affect Disord 61
7. Bechara A, Damasio H, Tranel D, Damasio AR (1997) Deciding advantageously before knowing the advantageous strategy. Science 275
8. Critchley HD, Garfinkel SN (2017) Interoception and emotion. Curr Opin Psychol 17:7–14
9. Parviainen T, Lyyra P, Nokia MS (2022) Cardiorespiratory rhythms, brain oscillatory activity and cognition: review of evidence and proposal for significance. Neurosci Biobehav Rev 142:104908
10. Boucsein W et al (2012) Publication recommendations for electrodermal measurements. Psychophysiology 49
11. Davis M, Walker DL, Miles L, Grillon C (2010) Phasic vs sustained fear in rats and humans: Role of the extended amygdala in fear vs anxiety. Neuropsychopharmacology 35
12. Grupe DW, Nitschke JB (2013) Uncertainty and anticipation in anxiety: An integrated neurobiological and psychological perspective. Nat Rev Neurosci 14
13. Lang PJ, Bradley MM, Cuthbert BN (1998) Emotion, motivation, and anxiety: brain mechanisms and psychophysiology. Biol Psychiatry 44:1248–1263

14. Garfinkel SN, Critchley HD, Pollatos O (2016) The interoceptive system: Implications for cognition, emotion, and health. in *Handbook of Psychophysiology, Fourth Edition* 10.1017/9781107415782.019
15. Paulus MP, Stein MB (2006) An Insular View of Anxiety. Biol Psychiatry 60
16. Dawson ME, Schell AM, Filion DL (2016) The electrodermal system. Handb Psychophysiol Fourth Ed. 10.1017/9781107415782.010
17. Lidberg L, Wallin BG (1981) Sympathetic Skin Nerve Discharges in Relation to Amplitude of Skin Resistance Responses. *Psychophysiology* 18
18. Sequeira H, Hot P, Silvert L, Delplanque S (2009) Electrical autonomic correlates of emotion. Int J Psychophysiol 71:50–56
19. Buzsaki G, Draguhn A (2004) Neuroscience Neuronal Oscillations in Cortical Networks. Science 304
20. Engel AK, Fries P, Singer W (2001) Dynamic predictions: oscillations and synchrony in top-down processing. Nat Rev Neurosci 2:704–716
21. Cavanagh JF, Frank MJ (2014) Frontal theta as a mechanism for cognitive control. Trends Cogn Sci 18:414–421
22. Stegmann Y, Teigeler J, Mirifar A, Keil A, Gamer M (2024) Electrocortical Responses in Anticipation of Avoidable and Inevitable Threats: A Multisite Study. J Neurosci 44
23. Klimesch W (2012) Alpha-band oscillations, attention, and controlled access to stored information. Trends Cogn Sci 16
24. Tzovara A, Korn CW, Bach DR (2018) Human pavlovian fear conditioning conforms to probabilistic learning. PLoS Comput Biol 14
25. Engel AK, Fries P (2010) Beta-band oscillations-signalling the status quo? Curr Opin Neurobiol 20
26. Sedley W, Cunningham MO (2013) Do cortical gamma oscillations promote or suppress perception? An under-asked question with an over-assumed answer. Front Hum Neurosci 7:595
27. Iotzov I et al (2017) Divergent neural responses to narrative speech in disorders of consciousness. Ann Clin Transl Neurol 4:784–792
28. Ring P et al (2021) Oscillatory brain activity associated with skin conductance responses in the context of risk. J Neurophysiol 126
29. Bach DR, Daunizeau J, Friston KJ, Dolan RJ (2010) Dynamic causal modelling of anticipatory skin conductance responses. Biol Psychol 85:163–170
30. Mobbs D et al (2007) When fear is near: Threat imminence elicits prefrontal-periaqueductal gray shifts in humans. Science 317
31. Fung BJ, Qi S, Hassabis D, Daw N, Mobbs D (2019) Slow escape decisions are swayed by trait anxiety. Nat Hum Behav 3
32. Qi S et al (2018) How cognitive and reactive fear circuits optimize escape decisions in humans. *Proc. Natl. Acad. Sci. U. S. A.* 115, 3186–3191
33. Kleckner IR et al (2017) Evidence for a Large-Scale Brain System Supporting Allostasis and Interoception in Humans. Nat Hum Behav 1:0069
34. Pessoa L (2017) A Network Model of the Emotional Brain. Trends Cogn Sci 21
35. Zubarev I, Zetter R, Halme HL, Parkkonen L (2019) Adaptive neural network classifier for decoding MEG signals. *NeuroImage* 197

36. Zubarev I, Vranou G, Parkkonen L, MNEflow (2022) Neural networks for EEG/MEG decoding and interpretation. SoftwareX 17:100951
37. Richter D, Ekman M, de Lange FP (2018) Suppressed sensory response to predictable object stimuli throughout the ventral visual stream. J Neurosci 38
38. Vuilleumier P, Armony JL, Driver J, Dolan RJ (2001) Effects of attention and emotion on face processing in the human brain: An event-related fMRI study. Neuron 30
39. Kamiński J, Brzezicka A, Gola M, Wróbel A (2012) Beta band oscillations engagement in human alertness process. Int J Psychophysiol 85
40. Mantini D et al (2011) Default mode of brain function in monkeys. J Neurosci 31
41. Raichle ME, Snyder AZ (2007) A default mode of brain function: A brief history of an evolving idea. NeuroImage 37:1083–1090
42. Ferraro S et al (2022) The central autonomic system revisited – Convergent evidence for a regulatory role of the insular and midcingulate cortex from neuroimaging meta-analyses. Neurosci Biobehav Rev 142:104915
43. Menon V, Uddin LQ (2010) Saliency, switching, attention and control: a network model of insula function. Brain Struct Funct 214
44. Craig AD (2009) How do you feel - now? The anterior insula and human awareness. Nat Rev Neurosci 10
45. Liberati G et al (2018) Gamma-band oscillations preferential for nociception can be recorded in the human insula. Cereb Cortex 28
46. Krystal AD (2024) Human Anterior Insular Cortex Encodes Multiple Electrophysiological Representations of Anxiety-Related Behaviors. 10.1101/2024.03.05.583610
47. Balban MY et al (2023) Brief structured respiration practices enhance mood and reduce physiological arousal. Cell Rep Med 4:100895
48. Mizuseki K, Sirota A, Pastalkova E, Buzsáki G (2009) Theta Oscillations Provide Temporal Windows for Local Circuit Computation in the Entorhinal-Hippocampal Loop. Neuron 64
49. Sperl MFJ et al (2019) Fear Extinction Recall Modulates Human Frontomedial Theta and Amygdala Activity. Cereb Cortex 29
50. Matthews SC, Paulus MP, Simmons AN, Nelesen RA, Dimsdale JE (2004) Functional subdivisions within anterior cingulate cortex and their relationship to autonomic nervous system function. *NeuroImage* 22
51. Spitzer B, Haegens S (2017) Beyond the status quo: A role for beta oscillations in endogenous content (RE)activation. *eNeuro* 4
52. Cornwell BR et al (2011) Anxiety overrides the blocking effects of high perceptual load on amygdala reactivity to threat-related distractors. Neuropsychologia 49
53. Lissek S et al (2014) Generalized anxiety disorder is associated with overgeneralization of classically conditioned fear. Biol Psychiatry 75
54. Craig AD (2005) Forebrain emotional asymmetry: A neuroanatomical basis? Trends Cogn Sci 9
55. Uddin LQ (2015) Salience processing and insular cortical function and dysfunction. Nat Rev Neurosci 16:55–61
56. Critchley HD (2002) Electrodermal responses: What happens in the brain. Neuroscientist 8
57. Bigalke JA, Carter JR (2022) Sympathetic Neural Control in Humans with Anxiety-related Disorders. Compr Physiol 12

58. Najström M, Jansson B (2007) Skin conductance responses as predictor of emotional responses to stressful life events. Behav Res Ther 45
59. Spielberger CD, Gorsuch RL, Lushene R, Vagg PR, Jacobs GA (1983) Manual for State–Trait Anxiety Inventory. Consulting Psychologists
60. Etkin A, Wager TD (2007) Functional neuroimaging of anxiety: A meta-ana lysis of emotional processing in PTSD, social anxiety disorder, and specific phobia. Am J Psychiatry 164
61. Etkin A, Büchel C, Gross JJ (2015) The neural bases of emotion regulation. Nat Rev Neurosci 16
62. Grillon C (2008) Models and mechanisms of anxiety: Evidence from startle studies. Psychopharmacology 199
63. Makowski D et al (2021) NeuroKit2: A Python toolbox for neurophysiological signal processing. Behav Res Methods 53
64. Greco A, Valenza G, Lanata A, Scilingo EP, Citi L (2016) CvxEDA: A convex optimization approach to electrodermal activity processing. IEEE Trans Biomed Eng 63
65. Fischl B, FreeSurfer (2012) *NeuroImage* 62
66. Taulu S, Simola J, Kajola M (2005) Applications of the signal space separation method. IEEE Trans Signal Process 53:3359–3372
67. Gramfort A et al (2013) MEG and EEG data analysis with MNE-Python. Front Neurosci 7
68. Hyvärinen A (1999) Fast and robust fixed-point algorithms for independent component analysis. IEEE Trans Neural Netw 10
69. Pascual-Marqui RD (2002) Standardized low-resolution brain electromagnetic tomography (sLORETA): technical details. Methods Find Exp Clin Pharmacol 24(Suppl D):5–12
70. Khan S et al (2018) Maturation trajectories of cortical resting-state networks depend on the mediating frequency band. NeuroImage 174:57–68
71. Haufe S et al (2014) On the interpretation of weight vectors of linear models in multivariate neuroimaging. NeuroImage 87:96–110
72. Bates D, Mächler M, Bolker B, Walker S (2015) Fitting linear mixed-effects models using lme4 [sparse matrix methods; linear mixed models; penalized least squares; Cholesky decomposition. J Stat Softw 67:1–48
73. Bell RM, Mccaffrey DF (2002) Bias Reduction in Standard Errors for Linear Regression with Multi-Stage Samples. Stat Can Cat No 28
74. Pustejovsky JE, Tipton E (2018) Small-Sample Methods for Cluster-Robust Variance Estimation and Hypothesis Testing in Fixed Effects Models. J Bus Econ Stat 36:672–683
75. Benjamini Y, Hochberg Y (1995) Controlling the False Discovery Rate: A Practical and Powerful Approach to Multiple Testing. J R Stat Soc Ser B Methodol 57:289–300
76. Davison AC, Hinkley DV (1997) Bootstrap Methods and Their Application. Cambridge University Press, Cambridge. 10.1017/CBO9780511802843

Figures

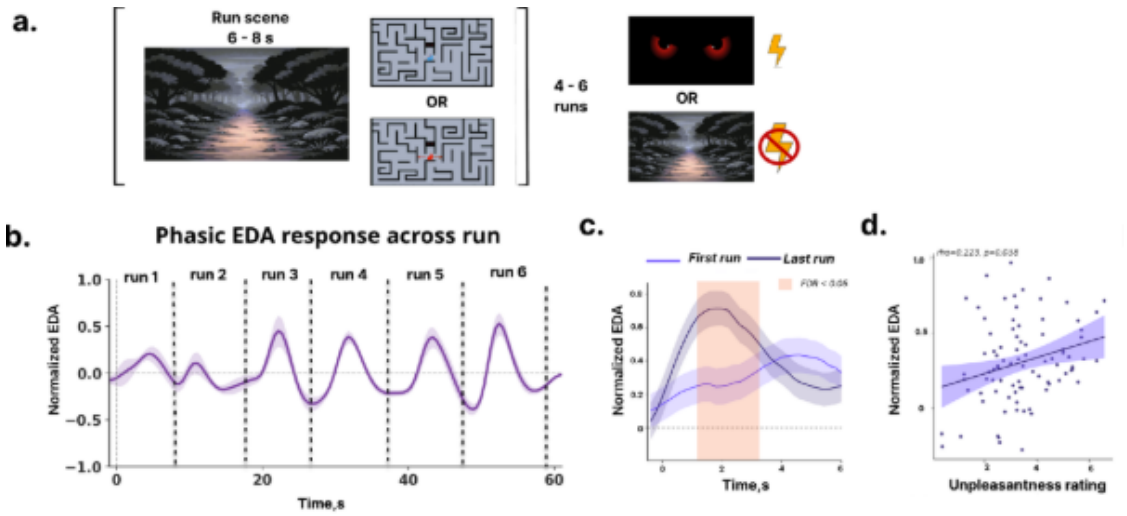


Figure 1

Phasic electrodermal responses increase across epochs and track subjective unpleasantness. (a) Experimental procedure; (b) Within-epoch rise in phasic EDA; (c) Increased EDA in first vs. last epochs; (d) EDA amplitudes correlation in last epochs averaged in 1.7 – 3 s after stimulus onset with trial-level unpleasantness ratings.

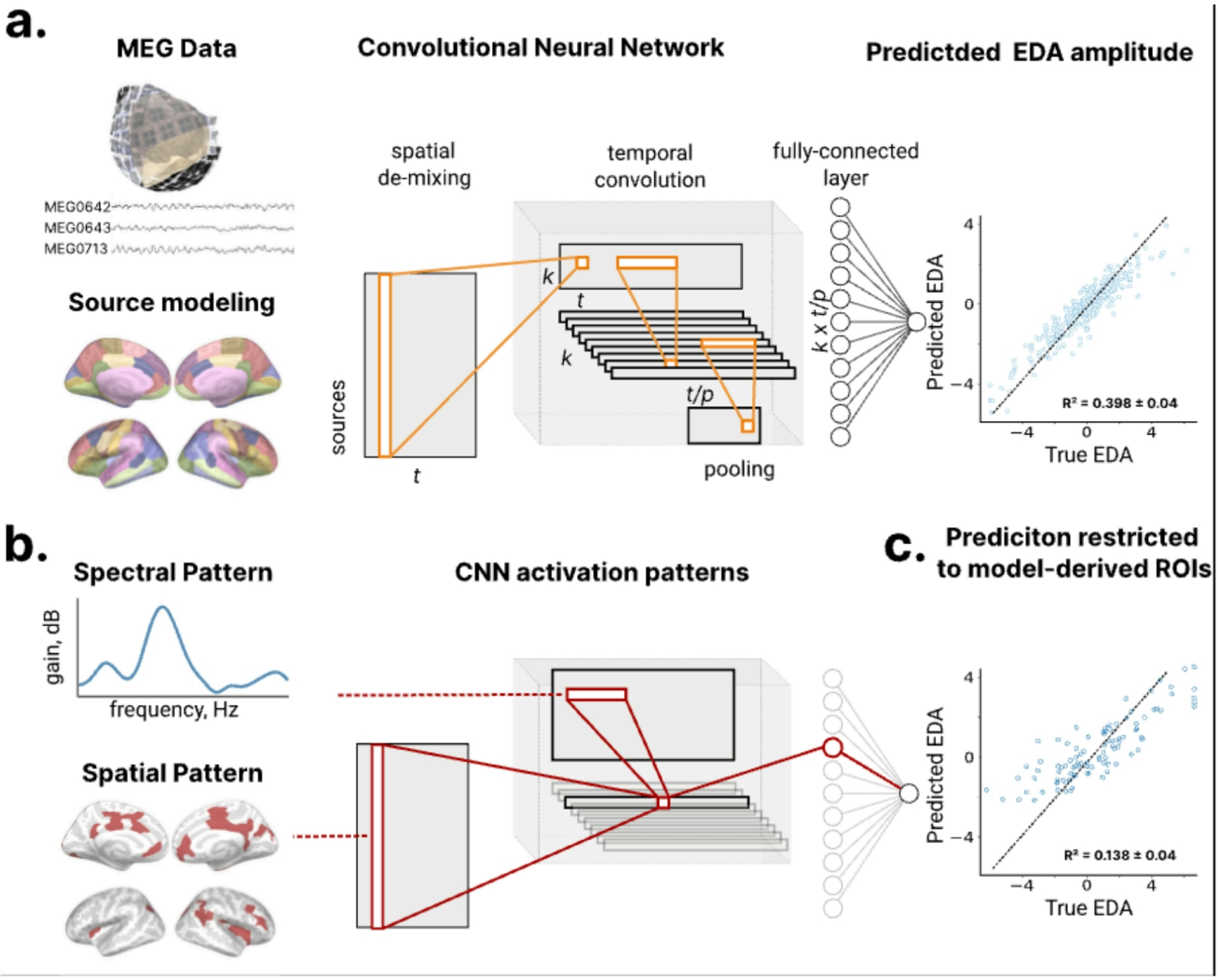


Figure 2

Deep-learning-derived spatial and frequency patterns predicting trial-by-trial sympathetic arousal.

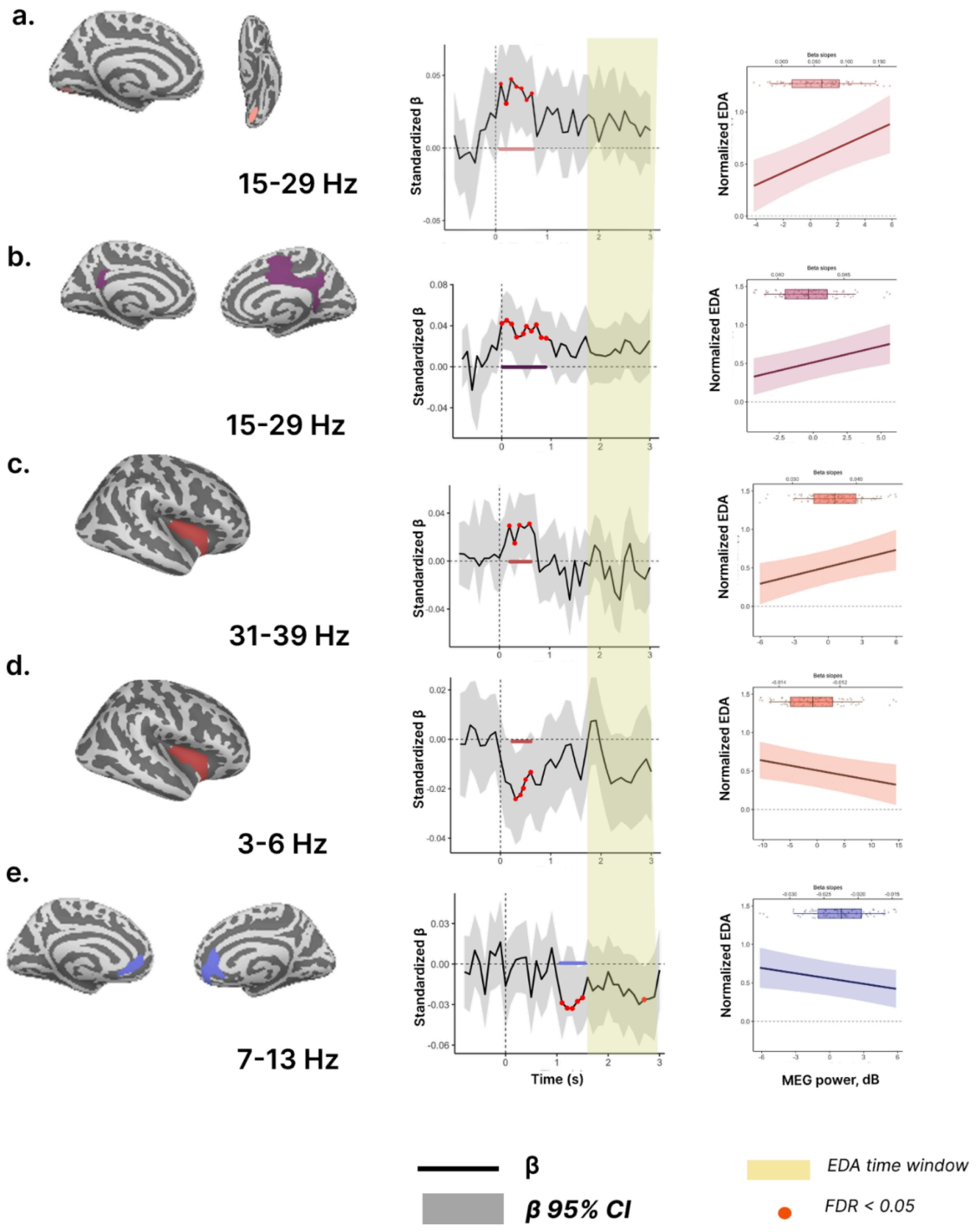


Figure 3

Time-resolved oscillatory predictors of sympathetic arousal across cortical regions.
*Left:*Regression slopes showing when oscillatory power predicts EDA. *Right:*Regression plot for significant time intervals and individual slopes variability.

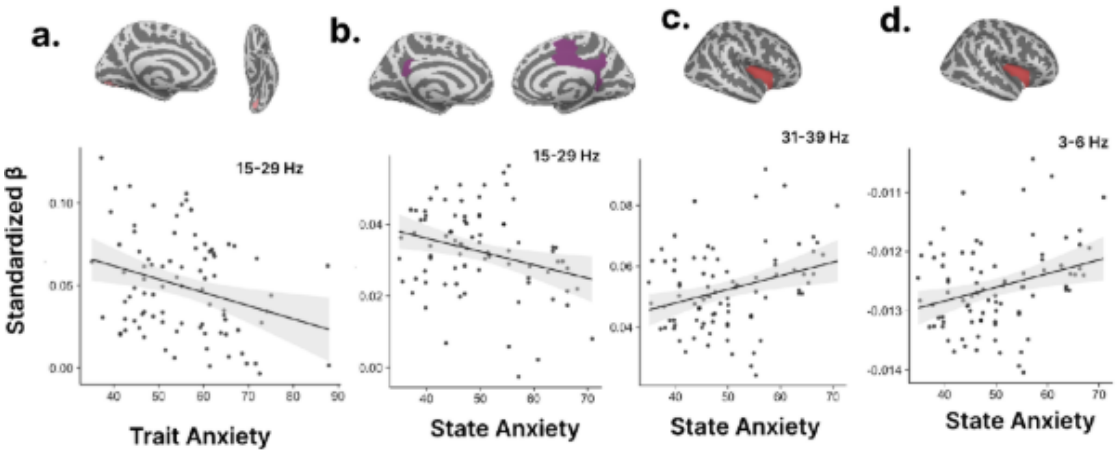


Figure 4

Correlation analysis within subject coefficients and trait and state anxiety

Supplementary Files

This is a list of supplementary files associated with this preprint. Click to download.

- COMMSBIO266762rs.pdf